Progress in Organic Coatings 77 (2014) 1554–1561

Contents lists available at ScienceDirect

Progress in Organic Coatings

journal homepage: www.elsevier.com/locate/porgcoat

Fluorescence study of film formation from PS/Al_2O_3 nanocomposites

Ö. Pekcan[a,*], Ş. Uğur[b], M.S. Sunay[c]

[a] Kadir Has University, Cibali, 34320 Istanbul, Turkey
[b] Istanbul Technical University, Department of Physics, Maslak, 34469 Istanbul, Turkey
[c] Piri Reis University, Faculty of Science and Letters, Tuzla, 34940 Istanbul, Turkey

ARTICLE INFO

Article history:
Available online 22 February 2014

Keywords:
Nanocomposites
Polystyrene
Annealing
Films
Fluorescence

ABSTRACT

Steady state fluorescence (SSF) and UV–vis (UVV) techniques were used to study the film formation behavior of pyrene (P) labeled polystyrene (PS) latex and Al_2O_3 (PS/Al_2O_3) composites depending on PS particles size and Al_2O_3 content. The close-packed arrays of PS spheres (SmPS: 203 nm; LgPS: 382 nm) templates on clean glass substrates were covered with various layers of Al_2O_3 by dip-coating method. Two different film series (SmPS/Al_2O_3 and LgPS/Al_2O_3) were prepared in various Al_2O_3 layer content. The film formation behavior of these composites were studied by annealing them at a temperature range of 100–250 °C and monitoring the scattered light intensity (I_{sc}), fluorescence intensity (I_P) from P and transmitted light intensity (I_{tr}) through the films after each annealing step. Optical results indicate that classical latex film formation was occurred for all Al_2O_3 content films and film formation process was unaffected by the Al_2O_3 content for both film series. Extraction of PS template produced highly ordered porous structures for high Al_2O_3 content in both film series. SEM images showed that the pore size and porosity could be easily tailored by varying the PS particle size and the Al_2O_3 content.

1. Introduction

As a result of worldwide theoretical and experimental efforts, a very good understanding of the mechanisms of latex film formation has been achieved [1–4]. Film formation from soft (low-T_g) and hard (high-T_g) latex dispersions can occur in several stages. In both cases, the first stage corresponds to the wet initial stage. Evaporation of solvent leads to second stage in which the particles form a close packed array, here if the particles are soft they are deformed to polyhedrons. Hard latex however stays undeformed at this stage. Annealing of soft particles causes diffusion across particle–particle boundaries which leads to a homogeneous continuous material. In the annealing of hard latex system, however, deformation of particles first leads to void closure [1–4] and then after the voids disappear diffusion across particle–particle boundaries starts, i.e. the mechanical properties of hard latex films evolve during annealing; after all solvent has evaporated and all voids have disappeared.

This understanding of latex film formation can now be exploited to underpin the processing of new types of coatings and development of new materials. Processing and microstructure development of ceramic and polymer coating prepared by depositing a solution or dispersion have been of interest in last few years [5,6]. Colloidal ceramics, sol–gel derived ceramics and polymers have been studied as coating systems. Organization of monodispersed colloidal particles like latex and silica microspheres into higher-order microstructures is attracting growing interest [7,8], since it provides unique structures suitable for various advanced devices and functional materials such as photonic crystals [9] and porous polymers [10]. Colloidal crystals consisting of three-dimensional ordered arrays of monodispersed spheres, represent novel templates for the preparation of highly ordered macroporous inorganic solids, exhibiting precisely controlled pore sizes and highly ordered three-dimensional porous structures. These features are requirements for new photonic crystals, and can be beneficial in catalysis or large-molecule separation processes by potentially improving mass transfer processes and efficiencies. Ordered arrays of polymer (e.g. polystyrene or poly(methyl methacrylate)) or silica nanospheres have been extensively studied in recent years for photonic crystal applications [11,12]. Recently, they have attracted renewed interest, mainly because they provide a much simpler, faster and cheaper approach than complex semiconductor nanolithography techniques to create 3D photonic crystals working in the optical wavelength range [13,14]. Photonic crystals (i.e. spatially periodic structures of dielectric materials with different refractive indices) have been extensively investigated worldwide. Because the lattice constant of photonic crystals is in the visible or infrared wavelength range, they can control the propagation of photons in a way similar to the way a semiconductor does for electrons.

* Corresponding author. Tel.: +90 212 5336532x1330; fax: +90 212 5332286.
E-mail address: pekcan@khas.edu.tr (Ö. Pekcan).

0300-9440/$ – see front matter © 2014 Elsevier B.V. All rights reserved.
http://dx.doi.org/10.1016/j.porgcoat.2013.10.017

Alumina is a very important inorganic material owning to its thermal, chemical, and mechanical stability, and the hierarchically porous alumina should be an attractive material which can be potentially used as catalyst supports, adsorbents, ion-exchange materials, membrane substrates, etc [15]. Several reports on porous alumina preparation can be found [16]. Al_2O_3 coatings have also become more popular for their high dielectric strength, exceptional stability, durability against hostile environments and high transparency down to 250 nm. During the last few years Al_2O_3 coatings have been widely used for their practical applications, such as refractory materials, antireflection coatings, highly anti corrosive materials [17], microelectronic devices [18], capacitance humidity sensors [19] and also in heat sinks in IC's and passivation of metal surfaces [20]. These films have been prepared by various techniques such as Spray pyrolysis [21], thermal evaporation [22], sputtering [23] etc.

In the present work, we report the preparation and characterization of PS/Al_2O_3 films. The film formation of these films was studied depending on PS particle size and Al_2O_3 content. The results indicate that LgPS/Al_2O_3 films showed complete film formation independent of Al_2O_3 content while no film formation occurred above a certain Al_2O_3 content for SmPS/Al_2O_3 films. The film formation stages were modeled and related activation energies were determined. After completion of film formation, PS templates were extracted with toluene. The resultant structure was the replica of the PS particles and the materials generated from this process exhibit remarkable ordering of the pores with different size.

2. Experimental

2.1. Materials

2.1.1. Polystyrene (latex) spheres

In this study, we used two types of PS latex with different diameters. The latex samples are composed of pyrene (P) labeled polystyrene. Fluorescent PS latexes were produced via emulsion polymerization process [24]. The polymerization was performed batch-wisely using a thermostatted reactor equipped with a condenser, thermocouple, mechanical stirring paddle and nitrogen inlet. Water (50 ml), Styrene monomer (3 g; 99% pure from Janssen) and the 0.014 g of fluorescent 1-pyrenylmethyl methacrylate (PolyFluor® 394) were first mixed in the polymerization reactor where the temperature was kept constant (at 70 °C). The water soluble radical initiator potassium persulfate (KPS) (1.6% wt/wt over styrene) dissolved in small amount of water (2 ml) was then introduced in order to induce styrene polymerization. Different surfactant sodium dodecyl sulfate (SDS) concentrations (0.03% and 0.12% wt/vol) were added in the polymerization recipe to change the particle size keeping all other experimental conditions the same. The polymerization was conducted under 400 rpm agitation during 12 h under nitrogen atmosphere at 70 °C. The particle size was measured using Malven Instrument NanoZS. The mean diameter of these particles is 203 nm (SmPS) and 382 nm (LgPS). The weight-average molecular weights (M_w) of individual PS chain (M_w) were measured by gel permeation chromatography (GPC) and found as 90×10^3 g mol^{-1} for both 203 nm (SmPS) and 382 nm (LgPS), respectively. The particle size of the polystyrene latex was decreased with increasing the concentration of SDS but its molecular weight remained almost unchanged with increasing SDS concentration. Glass transition temperature (T_g) of the PS latexes were determined using differential scanning calorimeter (DSC) and found to be around 105 °C. Fig. 1 shows the SEM images of SmPS and LgPS latex particles produced for this study.

2.1.2. Al_2O_3 solution

Al_2O_3 sol was prepared in the following way: A total of 2 ml aluminum-tri-*sec*-butoxide (Aldrich; 97%) was dissolved in 45 cm^3 water at 70 °C. The solution was stirred for 30 min. A small amount of acidic acid was continuously added as catalyst, until the solution became transparent and stirred for another 2 h. Oxide networks are formed upon hydrolytic condensation of alkoloxide precursors. Finally, a uniform and transparent Al_2O_3 sol was obtained for film fabrication.

2.2. Preparation of PS/Al_2O_3 films

Firstly, LgPS and SmPS aqueous suspensions were dropped on clean glass substrates and dried at room temperature. Upon slow drying at room temperature, powder LgPS and SmPS films were produced. In order to study the particle size effect of PS latex and Al_2O_3 content on film formation behavior of PS/Al_2O_3 composites, we prepared two series of films: *Series 1:* LgPS and Al_2O_3 (LgPS/Al_2O_3) and *Series 2:* SmPS and Al_2O_3 (SmPS/Al_2O_3).

Al_2O_3 sol was filled into the PS templates by dip-coating method. Here the Al_2O_3 content in the films was adjusted by consecutive dipping cycle. Seven different films for each series of films were produced with 0, 1, 3, 5, 8, 10, and 15 layers (dipping cycle) of Al_2O_3. In order to study the film formation behavior of PS/Al_2O_3 composites, the produced films were separately annealed above T_g of PS, at temperatures ranging from 100 to 250 °C. The temperature was maintained within ±2 °C during annealing. After each annealing step, films were removed from the oven and cooled down to room temperature.

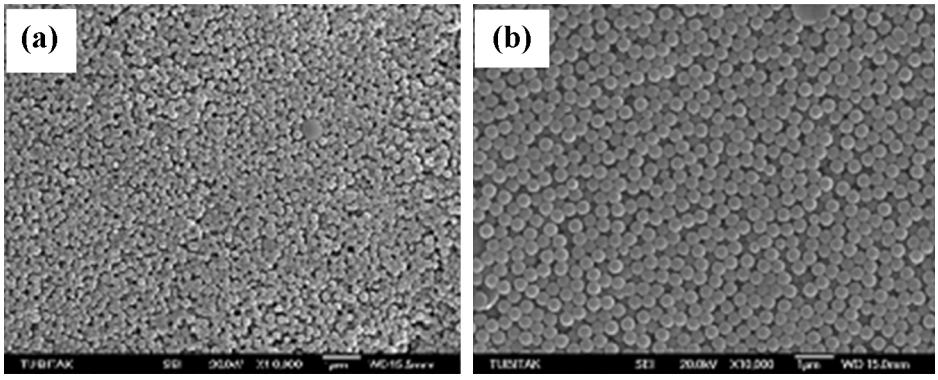

Fig. 1. SEM images of (a) SmPS and (b) LgPS latexes.

2.3. Methods

2.3.1. Fluorescence measurements

After annealing, each sample was placed in the solid surface accessory of a Perkin-Elmer Model LS-50 fluorescence spectrometer. Pyrene was excited at 345 nm and scattering and fluorescence emission spectra were detected between 300 and 500 nm. All measurements were carried out in the front-face position at room temperature. Slit widths were kept at 8 nm during all SSF measurements.

2.3.2. Photon transmission measurements

Photon transmission experiments were carried out using Carry-100 Bio UV–vis (UVV) scanning spectrometer. The transmittances of the films were detected at 500 nm. A glass plate was used as a standard for all UVV experiments, and measurements were carried out at room temperature after each annealing processes.

2.3.3. Scanning electron microscopy (SEM) measurements

Scanning electron micrographs of the PS/Al_2O_3 films were taken at 10–20 kV in a JEOL 6335F microscope. A thin film of gold (10 nm) was sputtered onto the surface of samples using a Hummer-600 sputtering system to help image the PS/Al_2O_3 films against the glass background.

3. Results and discussions

Figs. 2 and 3 show transmitted (I_{tr}), scattered (I_{sc}) and fluorescence (I_P) light intensities versus annealing temperatures for both SmPS/Al_2O_3 and LgPS/Al_2O_3 composite film series, respectively. Upon annealing the transmitted light intensity, I_{tr}, started to increase above a certain onset temperature, called the minimum film formation temperature T_0, for all film samples. Scattered light intensity showed a sharp increase at the single temperature named as the void closure temperature, T_v. Fluorescence intensity, I_P of all film samples first increase, reach a maximum, and then decrease with increasing annealing temperature [25,26]. The temperature where I_P reaches the maximum is called the healing temperature, T_h. Minimum film formation (T_0), void closure (T_v) and healing (T_h) temperatures are important characteristic related to the film formation properties of latexes. T_0 is often used to indicate the lowest possible temperature for particle deformation sufficient to decrease interstitial void diameters to sizes well below the wavelength of light [27]. Below this critical temperature, the dry latex is opaque and powdery. However, at and/or above this temperature, a latex cast film becomes continuous and clear film [28]. Here T_v is the lowest temperature at which I_{sc} become highest. The healing temperature (T_h) is the minimum temperature at which the latex film becomes continuous and free of voids. The healing point indicates the onset of the particle–particle adhesion [28]. Therefore, the increase in I_{tr} above T_0 can be explained by evaluation of the transparency of the composite films upon annealing. Most probably, increased I_{tr} corresponds to the void closure process [29]; i.e. polystyrene start to flow upon annealing and voids between particles can be filled. Since higher I_{tr} corresponds to higher clarity of the composite, then increase in I_{tr} predicts that microstructure of these films change considerably by annealing them, i.e. the transparency of these films evolve upon annealing. PS starts to flow due to annealing, and voids between particles can be filled due to the viscous flow. Further annealing at higher temperature causes healing and interdiffusion processes [26,29], resulting in a more transparent film.

The sharp increase in I_{sc} occurs at T_v, which overlaps the inflection point on the I_{tr} curve. Below T_v, light scatters isotropically because of the rough surface of the PS films. Annealing of the film at T_v creates a flat surface on the film, which acts like a mirror. As a result, light is reflected to the photomultiplier detector of the spectrometer. Further annealing makes the PS film totally transparent to light and I_{sc} drops to its minimum. On the other hand, the increase in I_P above T_0 presumably corresponds to

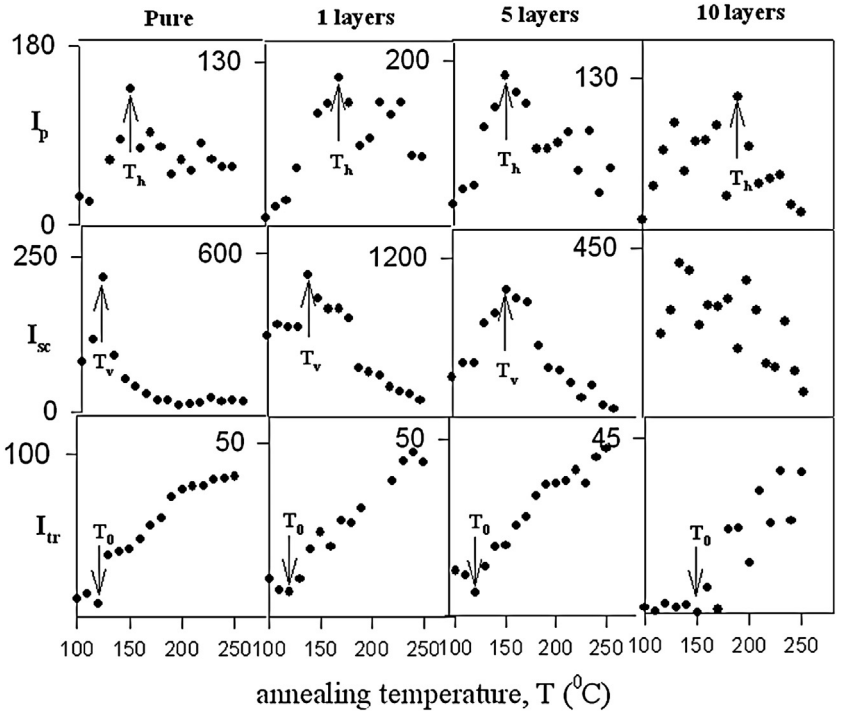

Fig. 2. Plot of I_{tr}, I_{sc} and I_P intensities versus annealing temperature, T for SmPS/Al_2O_3 composite films with 0 (pure), 1, 5 and 10 layers of Al_2O_3. Numbers on each curve shows Al_2O_3 content.

the void closure process up to the T_h point where the healing process takes place. Decrease in I_P above T_h can be understood by interdiffusion processes between polymer chains [30,31].

In order to determine the extent of film formation, films were soaked in toluene for 24 h to completely dissolve the PS template after the film formation is completed. After extraction of PS, the morphology of SmPS/Al_2O_3 films with one and five layers of Al_2O_3 (Fig. 4a) do not change significantly. In these images, SmPS spheres highly coated with Al_2O_3 are clearly seen. However, some spherical pores which must belong to the Al_2O_3 encapsulated replica of SmPS latexes are also observed. These pores have a well-pronounced circular shape and are isolated from each other. SEM image of the film prepared with 10 layers of Al_2O_3 in Fig. 4c shows an interconnected and open porosity with average pore size diameter of 203 nm, corresponding to approximately SmPS template diameter. In all images, besides the pores there are also voids that might be left by the interconnected SmPS aggregated spheres. It is understood that higher Al_2O_3 content and small PS size created a porous, disordered material after extraction of template.

On the other hand, SEM images of LgPS/Al_2O_3 composites given in Fig. 4b present highly porous structures after extraction process. The pores are uniformly distributed in space, but random pore morphology in the films with 1 and 5 layers of Al_2O_3 (see Fig. 4b) destroy their spherical shape. These films show a poorly ordered pore structure and heterogeneous pore-size distribution. For these low Al_2O_3 content films, a partially broken wall framework was obtained because the Al_2O_3 particles might not be sufficient to fully cover the surface of the LgPS template. However, it could be seen from Fig. 4b that film with 10 layers of Al_2O_3 shows well-defined spherical-ordered pores. The pores are uniformly distributed in the sample and showed an ordered connected porous structure. The homogenous distribution of the pores in the Al_2O_3 framework indicates that the porous structure retains the periodicity of the LgPS template.

In conclusion, SEM images of both film series showed that well defined open structure and interconnected porosity were obtained when Al_2O_3 content was increased. This behavior can be explained by removal of PS from the surface of the Al_2O_3 covered latex particles during the dissolution process. In other words, the film formation from SmPS and LgPS particles has occurred on top of the Al_2O_3 covered particles during annealing and, during dissolution, PS material is completely dissolved showing the microstructure of PS particles covered by Al_2O_3 layer. This picture is now depicted in Fig. 5 where the behavior of SmPS/Al_2O_3 and LgPS/Al_2O_3 composite films during annealing are presented [26]. In Fig. 5a, film posses many voids, which results in short mean-free and optical paths of a photon yielding very low I_P and I_{tr}. Fig. 5b shows a film in which interparticle voids disappear due to annealing, which gives rise to a long mean free and optical path in the film. At this stage, I_P and I_{tr} reach its maximum values. Finally, Fig. 5c presents almost transparent film with no voids but some Al_2O_3 background. At this stage, film has low I_P but high I_{tr} because the mean free path is very long but the optical path is short.

3.1. Film formation mechanisms

3.1.1. Void closure

In order to quantify the behavior of I_P below T_h and I_{tr} above T_0 in Figs. 2 and 3, a phenomenological void closure model can be introduced. Latex deformation and void closure between particles can be induced by shearing stress which is generated by surface tension of the polymer, i.e. polymer–air interfacial tension. The void closure kinetics can determine the time for optical transparency and latex film formation [32]. In order to relate the shrinkage of spherical void of radius, r, to the viscosity of the surrounding medium, η, an expression was derived and given by the following relation [32].

$$\frac{dr}{dt} = -\frac{\gamma}{2\eta}\left(\frac{1}{\rho(r)}\right) \quad (1)$$

where γ is the surface energy, t is time and $\rho(r)$ is the relative density. It has to be noted that here the surface energy causes a decrease

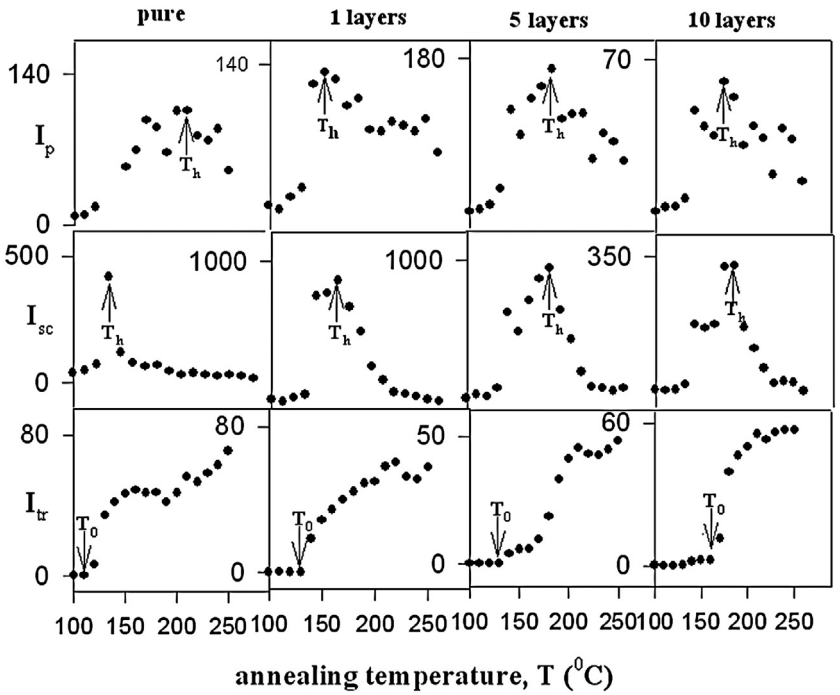

Fig. 3. Plot of I_{tr}, I_{sc} and I_P intensities versus annealing temperature, T for LgPS/Al_2O_3 composite films with 0 (pure), 1, 5 and 10 layers of Al_2O_3. Numbers on each curve shows Al_2O_3 content.

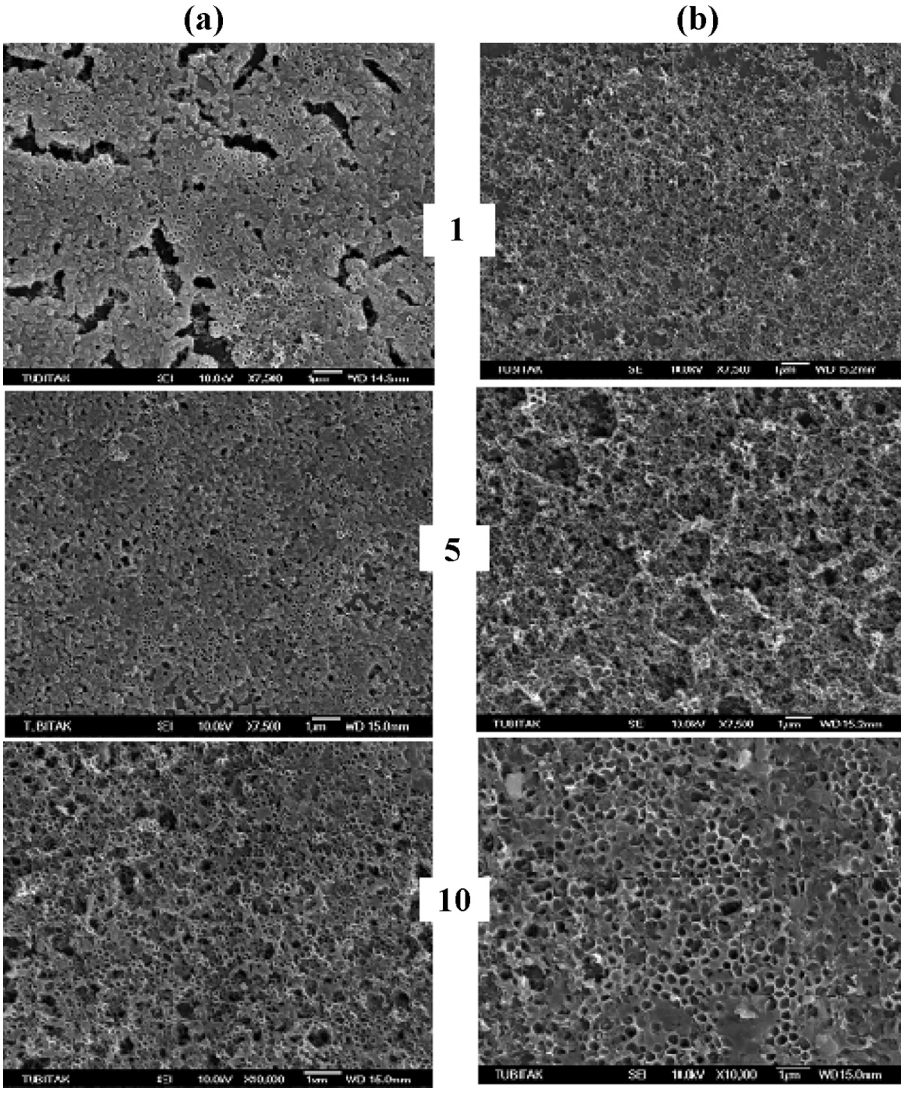

Fig. 4. SEM images of (a) SmPS/Al_2O_3 and (b) LgPS/Al_2O_3 composite films with 1, 5 and 10 layers of Al_2O_3 after extraction of PS template with toluene.

in void size and the term $\rho(r)$ varies with the microstructural characteristics of the material, such as the number of voids, the initial particle size and packing. Eq. (1) is similar to one that was used to explain the time dependence of the minimum film formation temperature during latex film formation [33,34]. If the viscosity is constant in time, integration of Eq. (1) gives the relation as

$$t = -\frac{2\eta}{\gamma}\int_{r_o}^{r}\rho(r)dr \tag{2}$$

where r_0 is the initial void radius at time $t = 0$. The dependence of the viscosity of polymer melt on temperature is affected by the overcoming of the forces of macromolecular interaction, which enables the segments of polymer chain to jump over from one equilibration position to another. This process happens at temperatures at which the free volume becomes large enough and is connected with the overcoming of the potential barrier. Frenkel–Eyring theory produces the following relation for the temperature dependence of viscosity [35,36]

$$\eta = \frac{N_0 h}{V}\exp\left(\frac{\Delta G}{kT}\right) \tag{3}$$

where N_0 is Avogadro's number, h is Planck's constant, V is molar volume and k is Boltzmann's constant. It is known that $\Delta G = \Delta H - T\Delta S$, so Eq. (3) can be written as

$$\eta = A \exp\left(\frac{\Delta H}{kT}\right) \tag{4}$$

where ΔH is the activation energy of viscous flow, i.e. the amount of heat which must be given to one mole of material to create the act of a jump during viscous flow; ΔS is the entropy of activation of viscous flow. Here A represents a constant for the related parameters that do not depend on temperature. Combining Eqs. (2) and (4), the following useful equation is obtained

$$t = -\frac{2A}{\gamma}\exp\left(\frac{\Delta H}{kT}\right)\int_{or}^{r}\rho(r)dr \tag{5}$$

In order to quantify the above results, Eq. (5) can be employed by assuming that the interparticle voids are equal in size and the

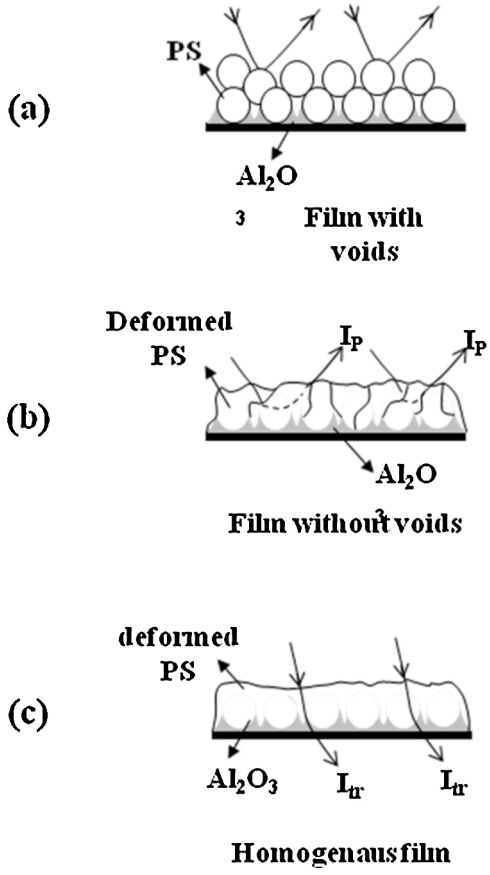

Fig. 5. Cartoon representation of PS/Al_2O_3 films at several annealing steps. (a) Film posses many voids that results in very low I_P and I_{tr}, (b) interparticle voids disappear due to annealing, I_P reaches its maximum value, and (c) transparent film with no voids but some Al_2O_3 background and has low I_P but high I_{tr}.

number of voids stays constant during film formation (i.e. $\rho(r) \approx r^{-3}$), Then integration of Eq. (5) gives the relation

$$t = \frac{2AC}{\gamma} \exp\left(\frac{\Delta H}{kT}\right)\left(\frac{1}{r^2} - \frac{1}{r_o^2}\right) \quad (6)$$

where C is a constant related to relative density $\rho(r)$. As we stated before, decrease in void size (r) causes an increase in I_P. If the assumption is made that I_P is inversely proportional to the 6th power of void radius, r, then Eq. (6) can be written as

$$t = \frac{2AC}{\gamma} \exp\left(\frac{\Delta H}{kT}\right)\left(I^{1/3}\right) \quad (7)$$

here r_o^{-2} is omitted from the relation since it is very small compared to r^{-2} values after void closure processes are started. Eq. (7) can be solved for I_P and I_{tr} (=I) to interpret the results in Figs. 2 and 3 as

$$I(T) = S(t) \quad \exp\left(-\frac{3\Delta H}{kT}\right) \quad (8)$$

where $S(t)=(\gamma t/2AC)^3$. For a given time the logarithmic form of Eq. (8) can be written as follows

$$\ln \quad I(T) = \ln \quad S(t) - \left(\frac{3\Delta H}{kT}\right) \quad (9)$$

As it was already argued above that, the increase in both I_P and I_{tr} originate due to the void closure process, then Eq. (9) was applied to I_{tr} above T_0 and to I_P below T_h for all film samples in two series. Fig. 6 presents the $\ln I_P$ versus T^{-1} and Fig. 7 presents $\ln I_{tr}$ versus T^{-1} plots for SmPS/Al_2O_3 film series from which ΔH_P and ΔH_{tr}

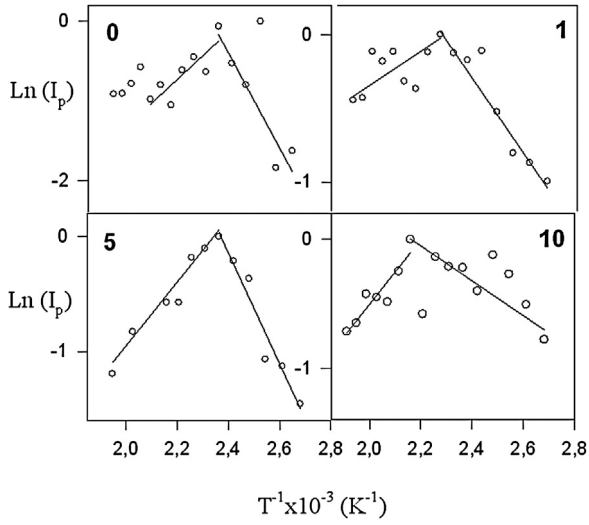

Fig. 6. The $\ln(I_P)$ versus T^{-1} plots of the data in Fig. 2 for SmPS/Al_2O_3 composite film contain (a) 0 (pure), (b) 1, (c) 5 and (d) 10 layers of Al_2O_3. The slope of the straight lines on right and left hand side of the graph produce ΔH_P and ΔE activation energies, respectively.

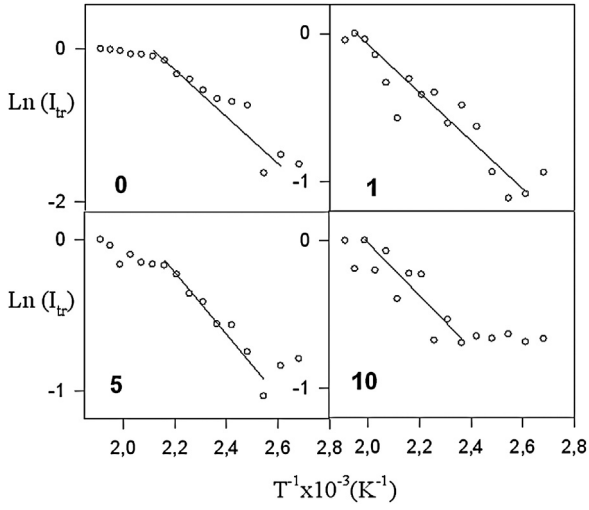

Fig. 7. The $\ln(I_{tr})$ versus T^{-1} plots of the data in Fig. 2 for SmPS/Al_2O_3 composite film contains (a) 0 (pure), (b) 1, (c) 5 and (d) 10 layers of Al_2O_3. The slope of the straight lines produces ΔH_{tr}.

activation energies were obtained. Similar fittings were also done for LgPS/Al_2O_3 film series and the measured ΔH_P and ΔH_{tr} activation energies are listed in Table 1 for both series. It is seen that ΔH_P values, except for pure SmPS and LgPS films, for both series do not change much by increasing the Al_2O_3 layer showing that the amount of heat that was required by one mole of polymeric material to accomplish a jump during viscous flow does not change by varying the Al_2O_3 layers on the latex films. In addition, ΔH_{tr} values of both film series also do not change much. It has to be noted that the measured activation energies for viscous flow process were found to be different in different techniques. This difference most probably originates from different techniques and second one measures the film formation from the inner latexes. Since pyrenes are labeled to PS chain, it is believed that ΔH_P values are more realistic to interpret the viscous flow. On the other hand, ΔH_{tr} values were obtained indirectly compared to ΔH_P values. When comparing the activation energies of both series, it is seen that ΔH values of LgPS/Al_2O_3 series are larger than those of SmPS/Al_2O_3 series. This implies that the viscous flow process is significantly affected by the PS particle

Table 1
Experimentally produced activation energies of $SmPS/Al_2O_3$ and $LgPS/Al_2O_3$ film series.

Al_2O_3 layer	$SmPS/Al_2O_3$			$LgPS/Al_2O_3$		
	ΔH_P (kcal mol^{-1})	ΔH_{tr} (kcal mol^{-1})	ΔE (kcal mol^{-1})	ΔH_P (kcal mol^{-1})	ΔH_{tr} (kcal mol^{-1})	ΔE (kcal mol^{-1})
0	2.5	2.2	7.5	2.2	10.6	12.6
1	1.2	0.8	3.2	3.1	8.2	3.6
3	1.7	0.6	3.4	2.2	4.9	5.8
5	2.2	1.0	7.7	3.0	6.1	7.1
8	2.7	0.8	6.0	2.5	7.2	4.6
10	0.9	0.8	10.0	2.2	6.7	8.7
15	1.5	1.1	7.8	2.4	8.3	5.1

size. With smaller diameter (i.e. 203 nm), the SmPS particles have larger surface area or surface free energy. The driving force for film formation is proportional to the inverse of the particle size, according to the descriptions of film formation driven by capillary forces [30]. The greater curvature and higher surface area of small particles are expected to encourage film formation. The specific surface area or the total surface energy of SmPS particles (diameter 203 nm) is much larger than that of LgPS particles (diameter 382 nm). As their total surface energy is much less than that of SmPS particles, LgPS particle requires higher energy to complete viscous flow process.

3.1.2. Healing and interdiffusion

The decrease in I_P was already explained in previous section, by interdiffusion of polymer chains. As the annealing temperature is increased above maxima, some part of the polymer chains may cross the junction surface and particle boundaries disappear, as a result I_P decreases due to transparency of the film. In order to quantify these results, the Prager–Tirrell (PT) model [37,38] for the chain crossing density can be employed. These authors used de Gennes's "reptation" model to explain configurational relaxation at the polymer–polymer junction where each polymer chain is considered to be confined to a tube in which executes a random back and forth motion [39] The total "crossing density" $\sigma(t)$ (chains per unit area) at junction surface then was calculated from the contributions $\sigma 1(t)$ due to chains still retaining some portion of their initial tubes, plus a remainder $\sigma 2(t)$ i. e. contribution comes from chains which have relaxed at least once. In terms of reduced time $\tau = 2\nu t/N^2$ the total crossing density can be written as [40]

$$\frac{\sigma(\tau)}{\sigma(\infty)} = 2\pi^{-1/2}\tau^{1/2} \tag{10}$$

where ν and N are the diffusion coefficient and number of freely jointed segment of polymer chain [37].

In order to compare our results with the crossing density of the PT model, the temperature dependence of $\sigma(\tau)/\sigma(\infty)$ can be modeled by taking into account the following Arrhenius relation for the linear diffusion coefficient

$$\nu = \nu_o \quad \exp\left(-\frac{\Delta E}{kT}\right) \tag{11}$$

here ΔE is defined as the activation energy for backbone motion depending on the temperature interval. Combining Eqs. (10) and (11) a useful relation is obtained as

$$\frac{\sigma(\tau)}{\sigma(\infty)} = R_o \quad \exp\left(-\frac{\Delta E}{2kT}\right) \tag{12}$$

where $R_o = (8\nu_o t/\pi N^2)^{1/2}$ is a temperature independent coefficient. The decrease in I_P in Figs. 2 and 3 above T_h is already related to the disappearance of particle–particle interface. As annealing temperature increased, more chains relaxed across the junction surface and as a result the crossing density increases. Now, it can be assumed that I_P is inversely proportional to the crossing density $\sigma(T)$ and then the phenomenological equation can be written as

$$I_P(\infty) = R_0^{-1} \quad \exp\left(\frac{\Delta E}{2k_BT}\right) \tag{13}$$

The activation energy of backbone motion, ΔE is produced by least-squares fitting the data in Fig. 6 (the left hand side) to Eq. (13) and are listed in Table 1. The ΔE values for each series seems almost not to change with increasing Al_2O_3 content showing that interdiffusion process is not affected by Al_2O_3 content. Furthermore, ΔE values for $LgPS/Al_2O_3$ series are slightly larger than that of $SmPS/Al_2O_3$ series. The polymer chains contain more free volume and less interaction between segments in SmPS particles leading to higher conformational energy and less interaction of polymer chains [31,41]. Polymer chains in the SmPS particle are in a highly confined state because of the spatial limitation compared to that of the random-coil state [31] in LgPS particles. This is the major reason for the SmPS particles need less energy to accomplish interdiffusion process in comparison with LgPS particles in composite films.

4. Conclusions

In this study, we employed the steady state fluorescence (SSF) technique in conjugation with UVV and SEM techniques to study film formation process of PS/Al_2O_3 nanocomposites and morphological changes depending on PS particle size and Al_2O_3 content. The results showed that film formation process of both composite film series was unaffected by the Al_2O_3 content since the film formation has occurred on top of the Al_2O_3 covered particles during annealing. However, activation energy values of $LgPS/Al_2O_3$ series were found slightly larger than $SmPS/Al_2O_3$ series which can be explained by PS size effect. Extraction of PS produced highly ordered porous structures for high Al_2O_3 content in both film series. The measurement obtained from the SEM showed that the pore size and porosity could be easily tailored by varying the PS particle size and the Al_2O_3 content. The results also showed that there is a good correspondence between the optical data and SEM images. These findings provide insight into the principle mechanism of latex film formation in inorganic oxide-based systems. Thus, our study presents useful informations and ideas about the kinetics of film formation in composite systems. On the other hand, similar observations was reported previously by Holland et al., where titania, zirconia, and alumina were used to construct highly ordered periodic 3D arrays of macro porous, using PS latex spheres as templates [42,43]. In Holland's work, corresponding metal alkoxide precursors permeate through PS spheres in room temperature, then close packed, open-pore structures with 320 to 360 nm voids were produced after calcinations of the organic component at 575 °C. Besides dip-coating and film formation modeling, the main difference between our work and their presentation comes from the dissolution of PS template using toluene to produce ordered pore structure from high Al_2O_3 content composites. In conclusion, the aim of both works is to produce highly structured metal oxides,

which could have applications in areas ranging from quantum electronics to photo catalysis to battery materials.

Acknowledgment

Dr. Sunay would like to thank the Laboratories in Physics Department of ITU, where she has done the experimental work during her Ph.D. studies, have used to prepare this manuscript.

References

[1] P.R. Sperry, B.S. Synder, M.L. O'Dowd, P.M. Lesko, Langmuir 10 (1994) 2619–2628.
[2] S. Mazur, Coalescence of polymer particles, in: N. Rosenweig (Ed.), Polymer Powder Processing, Wiley, New York, NY, 1995.
[3] J.K. Mackenzie, R. Shutlewort, Proc. Phys. Soc. 62 (1949) 833–852.
[4] J.W. Vanderhoff, Br. Polym. J. 2 (1970) 161–173.
[5] D.M. Vaessen, F.A. Ngantung, M.L.B. Palacio, L.F. Francis, A.V. McCormick, J. Appl. Polym. Sci. 84 (2001) 2784–2793.
[6] D.M. Vaessen, A.V. McCormick, L.F. Francis, Polymer 43 (2002) 2267–2277.
[7] D. Wang, H. Mohwald, J. Mater. Chem. 14 (2004) 459–468.
[8] A.D. Dinsmore, M.F. Hsu, M.G. Nikolaides, M. Marquez, A.R. Bausch, D.A. Weitz, Science 298 (2002) 1006–1009.
[9] E. Chomski, G.A. Ozin, Adv. Mater. 12 (2000) 1071–1078.
[10] J.H. Moon, S. Kim, G.-R. Yi, Y.-H. Lee, S.-M. Yang, Langmuir 20 (2004) 2033–2035.
[11] T. Yamasaki, T. Tsutsui, Appl. Phys. Lett. 72 (1998) 1957–1959.
[12] Yu.A. Vlasov, N. Yao, D.J. Norris, Adv. Mater. 11 (1999) 165–169.
[13] Y.A. Vlasov, X.Z. Bo, J.C. Sturm, D.J. Norris, Nature 414 (2001) 289–293.
[14] J. Wijnhoven, W.L. Vos, Science 281 (1998) 802–804.
[15] J. Sánchez-Valente, X. Bokhimi, F. Hernández, Langmuir 19 (2003) 3583–3588.
[16] Y. Tokudome, K. Fujita, K. Nakanishi, K. Miura, K. Hirao, Chem Mater. 19 (2007) 3393–3398.
[17] Dianran Yan, Jining He, Xiangzhi Li, Yangaia Liu, Jianxin Zhang, Huili Ding, Surf. Coat. Technol. 141 (2001) 1–6.
[18] Yi-Shung Chaug, Nripen Roy, Vac. Sci. Technol. 7 (1989) 1303–1304.
[19] R.K. Nahar, V.K. Khanna, Int. J. Electron. 52 (1982) 557–567.
[20] Yi-Shung Chaug, Nripen Roy, Thin Solid Films 193–194 (1990) 959–974.
[21] M. Aguiler-Fruits, M. Garcia, C. Falcony, G. Plesch, S. Jimenez-Sandoval, Thin Solid Films 389 (2001) 200–206.
[22] S. Mansour, A.I. Rob aee, G.N. Subbanna, K. Narasimha Rao, S. Mohan, Vacuum 45 (1994) 97–102.
[23] S. Maniv, W.D. Westwod, J. Vac. Sci. Technol. 17 (1980) 743–751.
[24] J.S. Liu, J.F. Feng, M.A. Winnik, J. Chem. Phys. 101 (1994) 9096–9103.
[25] M. Canpolat, Ö. Pekcan, J. Polym. Sci. Polym. Phys. Ed. 34 (1996) 691–698.
[26] S. Ugur, M.S. Sunay, A. Elaissari, F. Tepehan, O. Pekcan, Polym. Compos. 27 (2006) 651–659.
[27] J.L. Keddie, P. Meredith, R.A.L. Jones, A.M. Donald, Macromolecules 28 (1995) 2673–2682.
[28] S.T. Eckersley, A. Rudin, J. Coat. Technol. 62 (1990) 89–100.
[29] S. Ugur, A. Elaissari, O. Pekcan, J. Colloid Interface Sci. 263 (2003) 674–683.
[30] J.L. Keddie, Mater. Sci. Eng. R21 (1997) 101–170.
[31] C. Wu, K.K. Chan, K.F. Woo, R. Qian, X. Li, L. Chen, D.H. Napper, G. Tan, A.J. Hill, Macromolecules 28 (1995) 1592–1597.
[32] J.L. Keddie, P. Meredith, R.A.L. Jones, A.M. Donald, Film formation in waterborne coatings, in: T. Provder, M.A. Winnik, M.W. Urban (Eds.), ACS Symp. Ser. 648, American Chemical Society, 1996, pp. 332–348.
[33] G.B. Mc Kenna, in: C. Booth, C. Price (Eds.), Comprehensive Polymer Science, 2, Pergamon Press, Oxford, UK, 1989.
[34] H. Vogel, Phys. Z. 22 (1921) 645–646.
[35] G.S. Fulcher, J. Am. Ceram. Soc. 8 (1925) 339–355.
[36] J. Frenkel, Viscous flow of crystalline bodies under the action of surface tension, J. Phys. USSR 9 (1945) 385–391.
[37] S. Prager, M. Tirrell, J. Chem. Phys. 75 (1981) 5194–5198.
[38] R.P. Wool, B.L. Yuan, O.J. McGarel, J. Polym. Eng. Sci. 29 (1989) 1340–1367.
[39] P.G. de Gennes, J. Chem. Phys. 76 (1982) 3322–3326.
[40] Ö. Pekcan, E. Arda, Colloids Surf., A 153 (1999) 537–549.
[41] X. Qu, Y. Tang, L. Chen, X. Jin, Chin. Sci. Bull. 46 (2001) 991–996.
[42] B.T. Holland, C.F. Blanford, A. Stein, Science 281 (1998) 538–540.
[43] B.T. Holland, C.F. Blanford, A. Stein, M. Greenblatt, Chemtracts 12 (2) (1999) 121–124.